# Possible $\omega$ bound states in nuclei produced with the $(\gamma, p)$ reaction

M. Kaskulov,[1] H. Nagahiro,[2] S. Hirenzaki,[3] and E. Oset[1]
[1]*Departamento de Física Teórica and IFIC, Centro Mixto Universidad de Valencia-CSIC, Institutos de Investigación de Paterna, Aptd. 22085, E-46071 Valencia, Spain*
[2]*Research Center for Nuclear Physics, Osaka University, Ibaraki, Osaka 567-0047, Japan*
[3]*Department of Physics, Nara Women's University, Nara 630-8506, Japan*
(Received 24 October 2006; revised manuscript received 4 May 2007; published 26 June 2007)

We perform calculations for $\omega$ production in nuclei by means of the $(\gamma, p)$ reaction for photon energies and proton angles suited to currently running and future experiments in present laboratories. For some cases of possible $\omega$ optical potentials, we find that clear peaks are observable when a good resolution in the $\omega$ energy is available. We also study the inclusive production of $\pi^0\gamma$ in nuclei around the $\omega$ energy and find a double hump structure for the energy spectra, with a peak around a $\pi^0\gamma$ energy of $m_\omega - 100$ MeV, which could easily be misidentified by a signal of an $\omega$ bound state in nuclei, while it is actually due to a different scaling of the uncorrelated $\pi^0\gamma$ production and $\omega$ production with subsequent $\pi^0\gamma$ decay.

DOI: 10.1103/PhysRevC.75.064616 PACS number(s): 13.60.Le, 25.20.Lj, 36.10.Gv, 14.40.Cs

## I. INTRODUCTION

The interaction of hadrons with nuclei is one of the important chapters in hadron and nuclear physics, and much work has been devoted to it [1]. In particular, the behavior of vector mesons in nuclei has received much attention, stimulated by the ansatz of a universal scaling of the vector meson masses in nuclei suggested in Ref. [2] and the study of QCD sum rules in nuclei [3], although earlier studies within the Nambu-Jona-Lasinio model produced no dropping of the vector meson masses [4]. More concretely, the properties of the $\omega$ meson have been thoroughly studied theoretically, and different calculations have been carried out within varied models ranging from quark models to phenomenological evaluations or by using effective Lagrangians [5–23]. The values obtained for the self-energy of the $\omega$ in nuclei split nearly equally into attraction and repulsion and range from an attraction of the order of 100–200 MeV [9,11] to no changes in the mass [21] to a net repulsion of the order of 50 MeV [17].

Experimental work along these lines is also rich, and recently the NA60 Collaboration [24] has produced dilepton spectra of excellent mass resolution in heavy ion reactions, for the spectra of the $\rho$, which indicate a large broadening of the $\rho$ but no shift in the mass. It should be pointed out that other workers concluded from the study of dilepton formation in proton nucleus collisions [25] that the $\rho$ mass is shifted to lower energies, but this conclusion was criticized in Ref. [26], where no shift was seen for the $\rho$ mass from the study of dilepton formation in photon nucleus collisions. As shown in Ref. [26], the different conclusions can be traced back to the choice of background.

It has been argued in Ref. [27] that reactions involving the interaction of elementary particles with nuclei can be as good as those with heavy ion collisions to show the medium effects of particles, with the advantage of being easier to analyze. In this sense, a variety of experiments have been done with $pA$ collisions in nuclei at KEK [25,28–30] and with photonuclear collisions at Jefferson Lab [26,31] by looking at dilepton spectra, including those discussed above.

A different approach has been followed by the CB-ELSA/TAPS Collaboration by looking at the $\gamma\pi^0$ coming from the $\omega$ decay. In this line, a recent work [32] claims to show evidence for a decrease of the $\omega$ mass in the medium of the order of 100 MeV from the study of the modification of the mass spectra in $\omega$ photoproduction (actually, the conclusions of this paper are tied to the way the background is subtracted, and it is shown in Ref. [33] that with other justified choices of background there is no need for a mass shift).

With sufficient attraction, $\omega$ bound states could be produced and could even be observable provided the $\omega$ width in the medium were not too large. Indeed, several works have investigated the possibility of having $\omega$ bound states in nuclei [9,34], and speculations on this possibility are also exploited in Ref. [35]. Suggestions to measure such possible states with the $(d$,He-3) recoilless reaction have also been made [36].

In the present work, and stimulated by the work of Ref. [35], we shall study the photon-induced $\omega$ production in nuclei, looking at the experimental setup of Ref. [35] as well as other setups which we consider more suited to observing bound $\omega$ states with this reaction. We will make predictions for cross sections for the $(\gamma, p)$ reaction in nuclei, leading to $\omega$ bound states, for several photon energies and proton angles.

At the same time, we will present results for inclusive $\omega$ production, looking at the $\gamma\pi^0$ decay mode of the $\omega$, as in Ref. [35], and we will show that because of the presence of an unavoidable background of $\gamma\pi^0$ (unrelated to the $\omega$) at $\gamma\pi^0$ energies smaller than the $\omega$ mass, and because of the different $A$-mass dependence of the background and $\omega$ production, a peak develops around $m_\omega - 100$ MeV in nuclei, which we warn must not be misidentified by a signal of a bound $\omega$ state in the nucleus. We will also show the optimal conditions for observing signals of eventual $\omega$ bound states, as well as the minimal experimental resolution necessary to see the possible peaks.

 

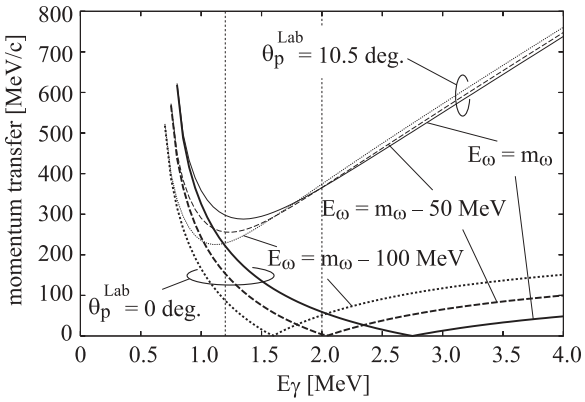


FIG. 1. Momentum transfers as a function of the incident photon energy $E_\gamma$ in the $(\gamma, p)$ reaction. The solid, dashed, and dotted lines show the momentum transfers at $\omega$ energy $E_\omega = m_\omega$, $E_\omega = m_\omega - 50$ MeV, and $E_\omega = m_\omega - 100$ MeV, respectively. The thick lines indicate the forward reaction cases; the thin lines, the cases for the ejected proton in the final state with the finite angle $\theta_p^{\rm Lab} = 10.5^\circ$. The vertical dashed lines show the incident energies $E_\gamma = 1.2$ and 2.0 GeV.

## II. PRODUCTION OF $\omega$ BOUND STATES IN THE $(\gamma, p)$ REACTION

Here we evaluate the formation rate of $\omega$ bound states in the nucleus by means of the $(\gamma, p)$ reaction. We use the Green's function method [37] to calculate the cross sections for $\omega$-mesic state formation as described in Refs. [38,39] in detail. The theoretical model used here is exactly the same as that used in those references.

We show first the momentum transfer of the $(\gamma, p)$ reaction in Fig. 1 as a function of the incident photon energy, at forward and finite angles of the emitted proton. The momentum transfer is the important kinematic variable which determines the experimental feasibility of the formation of meson-nuclear bound states. Indeed, deeply bound pionic atoms were discovered experimentally at the recoilless kinematics [36,40–42]. In the formation of $\omega$ states, we find that the recoilless condition is satisfied at $E_\gamma \sim 2.7$ GeV, as in Ref. [34], for $\omega$ production at threshold and forward proton production. However, the recoilless condition is never satisfied for finite proton angles. Since some experimental setups can have problems in proton forward detection, it is interesting to determine the optimal conditions with these boundary conditions. For this purpose, we look at the optimal photon energy for protons emitted with a finite angle. For an angle of $\theta_p^{\rm lab} = 10.5^\circ$ for the emitted proton, the angle measured in Ref. [35], the momentum transfer takes the minimum value at $E_\gamma \sim 1.2$ GeV. In this section, we consider 1.2 and 2.0 GeV as the incident photon energies and $0^\circ$ and $10.5^\circ$ as the emitted proton angles in the laboratory frame.

To calculate the cross sections at finite angles of the emitted proton, we estimate the elementary cross sections from the experimental data shown in Tables 3–5 in Ref. [43], and we use 5.0 $\mu$b/sr ($\theta_p^{\rm Lab} = 0^\circ$) and 8.0 $\mu$b/sr ($10.5^\circ$) at $E_\gamma = 1.2$ GeV, and 0.7 $\mu$b/sr for both $\theta_p^{\rm Lab} = 0$ and $10.5^\circ$ at $E_\gamma = 2.0$ GeV in the laboratory frame, respectively.

The $\omega$-nucleus optical potential is written here as

$$V(r) = (V_0 + iW_0)\frac{\rho(r)}{\rho_0}, \tag{1}$$

where $\rho(r)$ is the nuclear experimental density for which we take the two-parameter Fermi distribution. We consider three cases of the potential strength (in MeV) as

$$(V_0, W_0) = -(0, 50), \tag{2a}$$
$$= -(100, 50), \tag{2b}$$
$$= -(156, 29). \tag{2c}$$

The reason for these choices is as follows. From Ref. [35] on the $\omega$ production rates in different nuclei, one deduces a width for $\omega$ at the average $\omega$ momentum in the production ($\sim$900 MeV) and $\rho = \rho_0$ of about 100 MeV [44]. This means that the imaginary part of the potential has a strength of about 50 MeV. The momenta of the $\omega$ in a possible $\omega$ bound state would be of the order of 100–150 MeV, hence we should keep the door open to the possibility that, because of a particular momentum dependence, the imaginary part of the $\omega$ optical potential would be smaller for smaller momenta. For this reason we also investigate the case of Eq. (2c) with the $\omega$ width of 58 MeV at $\rho = \rho_0$. As discussed above, uncertainties in the subtraction of background in the experiment of Ref. [32] do not allow us to draw any conclusions on the shift of the mass [33]. Thus we have kept open the possibility of a downward mass shift and have performed calculations for 100 MeV binding, too. We also consider the potential estimated theoretically shown in Eq. (2c), which is obtained by the linear density approximation with the scattering length $a = 1.6 + 0.3i$ fm [11]. This potential in Eq. (2c) is strongly attractive with weak absorption and hence should be the ideal case for the formation of $\omega$ mesic nuclei.

No $\omega$ bound states are expected for the potential in Eq. (2a) which has only an absorptive part. The potential in Eq. (2b) has a strong attraction with the large absorptive part as indicated in Ref. [35]. It is also interesting to compare the formation spectra obtained with the potentials in Eqs. (2b) and (2c) to know the effects of the $\omega$ absorption in nuclei.

We should mention here that all the spectra in this section are plotted as functions of $E_\omega - m_\omega$, while in previous papers [36,38–41] they were plotted as functions of excitation energies of final mesic-nuclear states, or equivalently, the energies of emitted particles which also included the excitation energies of the core nucleus. We plot the spectra in this manner since we assume here experiments in which the $\omega$ meson energy can be deduced separately from the nuclear core excitation. This is the case here, where the $\omega$ energy is measured by the $\pi^0$ and $\gamma$ observations from the subsequent $\omega$ decay, $\omega \to \pi^0\gamma$, in the nucleus. We also take into account the realistic experimental energy resolution in the results.

First, we show in Fig. 2 the calculated results at $E_\gamma = 2.0$ GeV with the potential in Eq. (2c). As described above, this potential is one of the ideal cases for obtaining sharp signals for the mesic state formation. As we can see in Fig. 2(a), the peaks due to the mesic-nucleus formation can be seen clearly in the spectra at $\theta_p^{\rm Lab} = 0^\circ$, where the momentum transfer is small as shown in Fig. 1, and the spectra are similar to

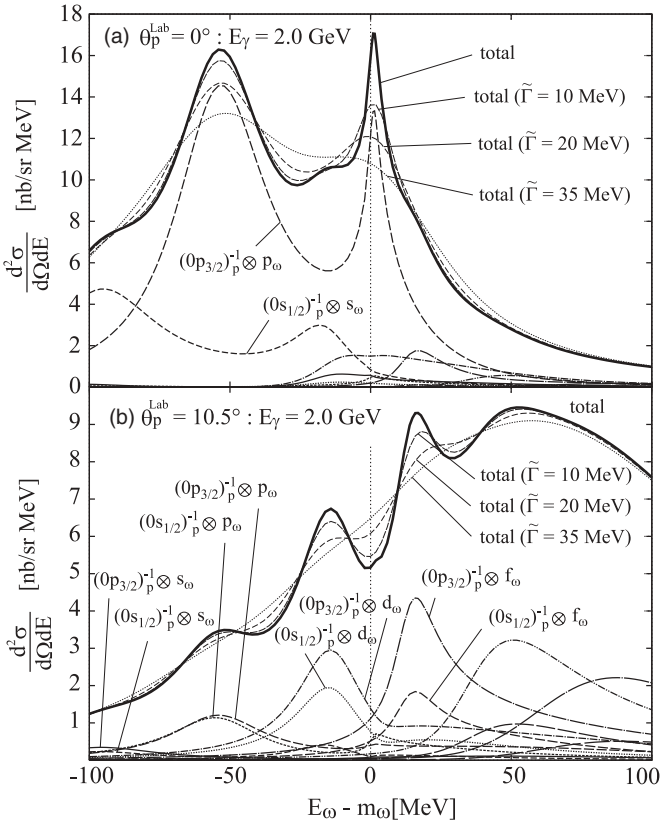


FIG. 2. Formation spectra of the $\omega$ mesic nucleus in $^{12}C(\gamma, p)$ reaction at emitted proton angle (a) $\theta_p^{Lab} = 0°$ and (b) $\theta_p^{Lab} = 10.5°$ calculated with the potential depth $(V_0, W_0) = -(156, 29)$ MeV as in Eq. (2c). The incident photon energy is $E_\gamma = 2.0$ GeV. The thick solid lines show the total spectra; the dashed lines, the subcomponents as indicated in the figures. The assumed experimental resolutions $\tilde{\Gamma}$ are also indicated.

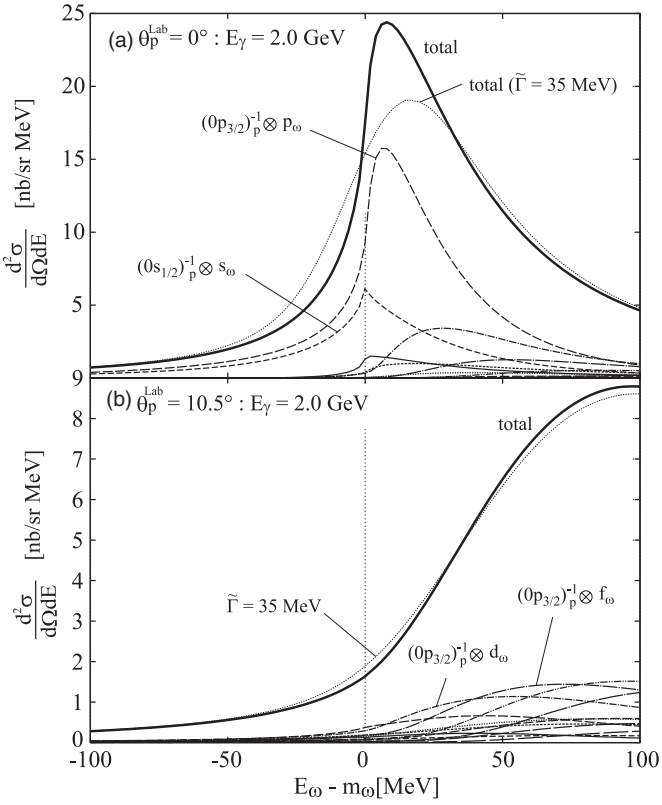


FIG. 3. Same as Fig. 2, except for the potential depth $(V_0, W_0) = -(0, 50)$ MeV as in Eq. (2a).

those obtained in Ref. [34] as expected. Only a limited number of subcomponents corresponding to the substitutional states are important in this case as a consequence of the recoilless kinematics. In the spectra, we can clearly identify the $\omega$ mesic $2p$ state around $E_\omega - m_\omega = -50$ MeV.

On the other hand, we found the spectra with significantly different shapes at $\theta_p^{Lab} = 10.5°$ as shown in Fig. 2(b). Because of the large momentum transfer around 350 MeV/$c$ at this proton angle, many subcomponents have finite contributions to form the total spectrum, as shown in Fig. 2(b), and the $\omega$ production spectrum is more similar to a continuum, although only the excitation of discrete nuclear states is considered in our calculations. The signals of the mesic bound states are now smaller than those at 0°. Thus, it is clear that the experiments at $\theta_p^{Lab} = 0°$ are better suited than those at finite angles to look for the signals of $\omega$ mesic bound states at $E_\gamma = 2.0$ GeV.

In Fig. 2, we also show the expected spectra with finite experimental energy resolutions $\tilde{\Gamma}$. We implement this experimental resolution in our calculations by convoluting the theoretical curves with a Gaussian distribution of width $\tilde{\Gamma}$, which is the width of the distribution at half its maximum strength. The energy resolution is estimated to be around 35–50 MeV in a realistic case [35]. We find in the figures that the peak structures in the spectrum with the potential (2c) almost disappeared for larger experimental resolutions than $\tilde{\Gamma} =$ 10 MeV. Thus, we conclude that an energy resolution better than 20 MeV is essentially required to obtain experimental evidence of the existence (or nonexistence) of the $\omega$ mesic nucleus.

In Figs. 3 and 4, we show the calculated spectra with the potentials in Eqs. (2a) and (2b) at $E_\gamma = 2.0$ GeV. For the potential (2a) case, we can see in Fig. 3(a) the enhancement of the cross section at $\theta_p^{Lab} = 0°$ around $E_\omega - m_\omega = 0$ MeV. In this case, bound states do not exist and the enhancement is due to the excitation of the $\omega$ to the continuum with recoilless kinematics. At $\theta_p^{Lab} = 10.5°$, the enhancement is removed by the kinematic conditions with the larger momentum transfer as shown in Fig. 3(b). In Fig. 4, the spectra with potential (2b) are shown for $\theta_p^{Lab} = 0°$ and 10.5°. In this case, the real part of the optical potential has enough attraction to form the bound states in the nucleus; however, the imaginary part of the optical potential is also strong enough to provide a large decay width for these bound states. Thus, we can see in Fig. 4(a) that there exists a certain strength under the threshold energy which includes the contributions of the bound state formations; however, we cannot identify the binding energies or the widths from the spectra due to the large width of the bound states. At $\theta_p^{Lab} = 10.5°$, we can only see a smooth slope in the spectra.

We next consider the cases with lower incident energy at $E_\gamma = 1.2$ GeV, where the momentum transfer at $\theta_p^{Lab} = 10.5°$ takes the smallest value as shown in Fig. 1. Theoretical

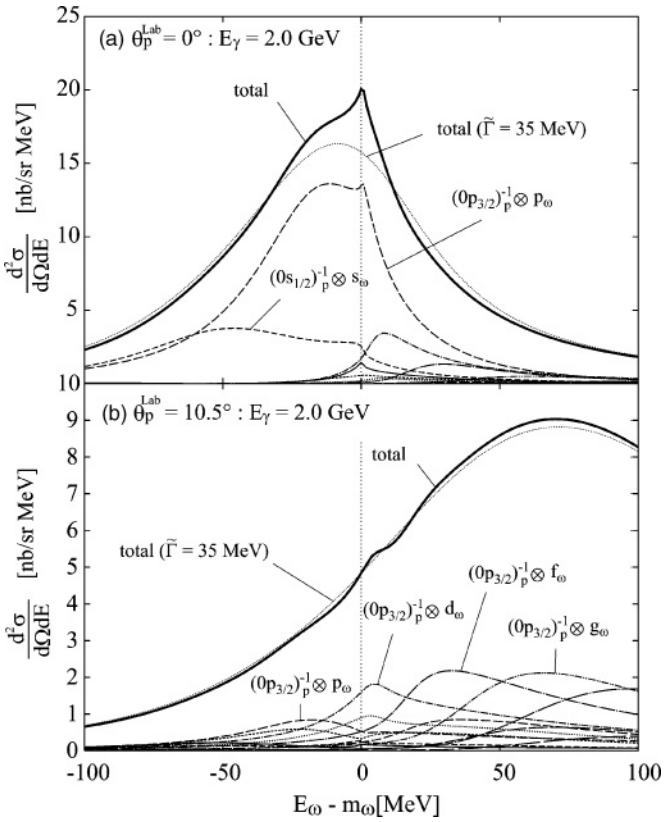


FIG. 4. Same as Fig. 2, except for the potential depth $(V_0, W_0) = -(100, 50)$ MeV as in Eq. (2b).

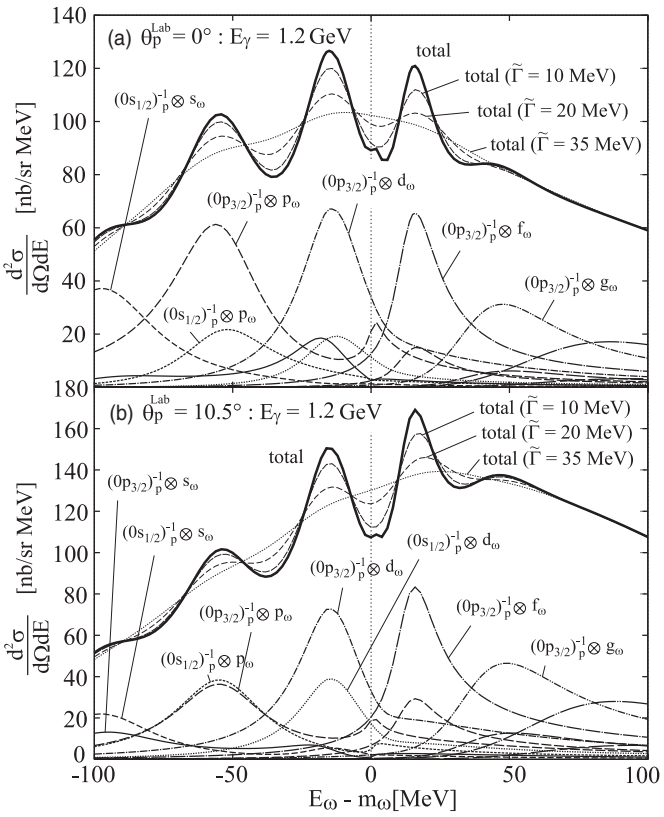


FIG. 5. Formation spectra of the $\omega$ mesic nucleus in $^{12}C(\gamma, p)$ reaction at emitted proton angle (a) $\theta_p^{Lab} = 0°$ and (b) $\theta_p^{Lab} = 10.5°$ calculated with the potential depth $(V_0, W_0) = -(156, 29)$ MeV as in Eq. (2c). The incident photon energy is $E_\gamma = 1.2$ GeV. The thick solid lines show the total spectra; the dashed lines, the subcomponents as indicated in the figures. The assumed experimental resolutions are also indicated.

investigations of this kinematics should be important to the design of experiments which have difficulties for the forward observation [35]. In Fig. 5, we show the results with the potential (2c) at this photon energy. As shown in Fig. 1, since the momentum transfer at 0° is smaller than at 10.5°, the signals can be seen clearer at 0° in Fig. 5(a) than at 10.5° in Fig. 5(b), as expected. However, we think it is more important to compare the spectrum in Fig. 5(b) at 1.2 GeV with that in Fig. 2(b) at 2.0 GeV to know the better suited incident energy for the observation at finite angles of the emitted proton. We should stress that even if 2.0 GeV allows a smaller momentum transfer than 1.2 GeV when the proton is measured forward, the signals are clearer in the spectrum at 1.2 than at 2.0 GeV at $\theta_p^{Lab} = 10.5°$, since the momentum transfer is smaller for the lower incident photon energy. In any case, a better experimental energy resolution than about 20 MeV is required to obtain decisive information from data on the $\omega$ mesic-nucleus as mentioned above.

In Figs. 6 and 7, we also show the calculated spectra with potentials (2a) and (2b) at $E_\gamma = 1.2$ GeV. As can be seen in these figures, the spectra show a smooth $\omega$ energy dependence at this photon energy, and the spectra at 0° and 10.5° resemble each other.

As a summary of this section, we would like to add few comments. To obtain the new information on the $\omega$ mesic nucleus, we need to have the data measured with sufficiently good energy resolution, otherwise we cannot make a conclusion as to the existence or nonexistence of the signals due to the mesic-nucleus formation. Furthermore, when planning to perform experiments, it is useful to consider the kinematic conditions carefully. In the cases studied here, the incident photon energy $E_\gamma = 2.0$ GeV is better suited for experiments detecting proton emission at $\theta_p^{Lab} = 0°$, while the lower photon energy $E_\gamma = 1.2$ GeV is better suited for finite angle proton emission at $\theta_p^{Lab} = 10.5°$.

## III. MONTE CARLO SIMULATION OF THE REACTION $\gamma A \to \pi^0 \gamma X$

In this section, we perform the Monte Carlo (MC) computer simulation of the inclusive $A(\gamma, \omega \to \pi^0\gamma)X$ reaction from different nuclei. The method used here (see details in Ref. [33]) combines a phenomenological calculation of the intrinsic probabilities for different nuclear reactions, such as the quasielastic and absorption channels, as a function of the nuclear matter density, with a computer MC simulation procedure in order to trace the fate of the $\omega$ meson and its decay products $\pi^0\gamma$ in the nuclear medium. Because our MC calculations represent complete event simulations it will be possible to take into account the actual experimental acceptance effects. In the following, we will carry out the

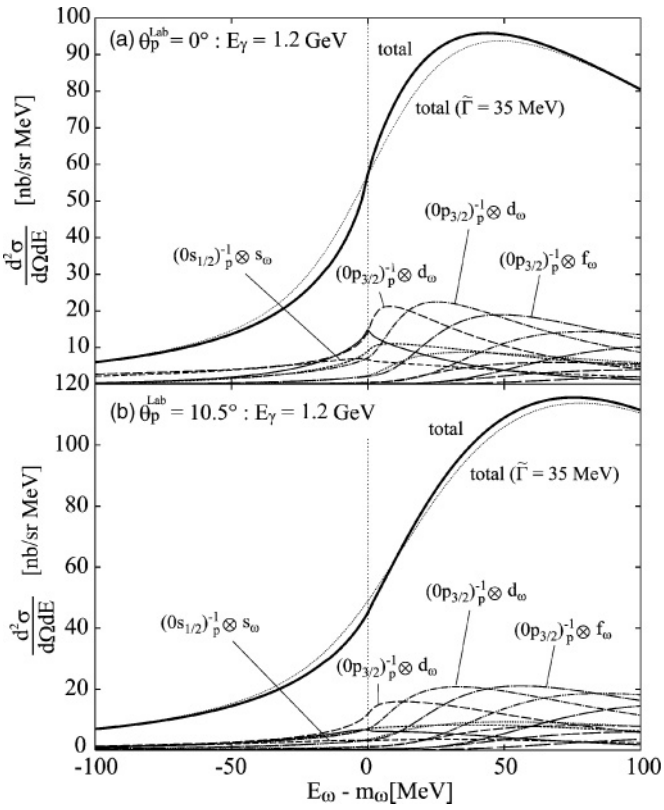


FIG. 6. Same as Fig. 5, except for the potential depth $(V_0, W_0) = -(0, 50)$ MeV as in Eq. (2a).

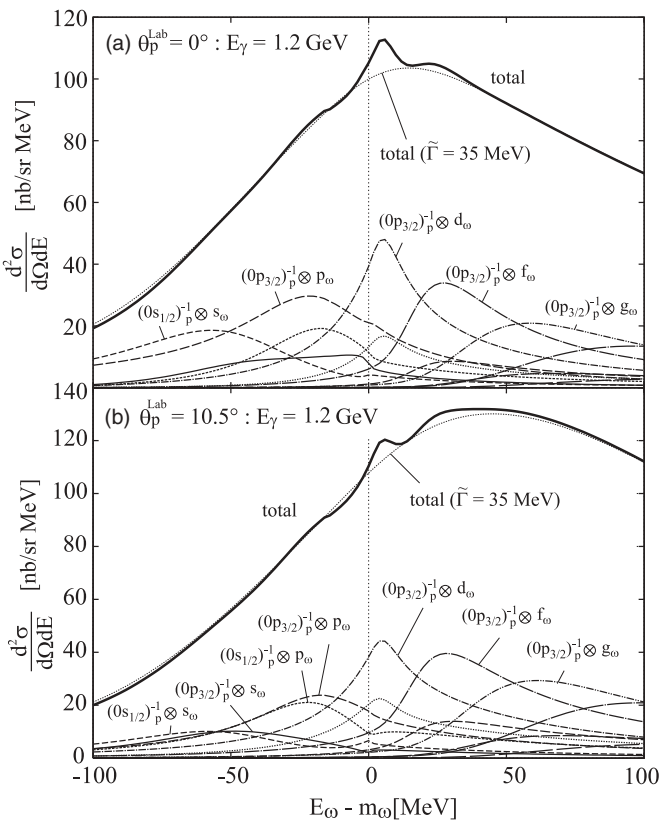


FIG. 7. Same as Fig. 5, except for the potential depth $(V_0, W_0) = -(100, 50)$ MeV as in Eq. (2b).

MC simulation taking into account the actual geometric and kinematic acceptance conditions of the TAPS/Crystal Barrel experiment at ELSA [35].

The content of this section is qualitative. We do not aim at giving precise cross sections of $\omega$ production or understanding the sources of background. The study is only made to show that certain characteristics can appear in the reactions in nuclei that have a conventional origin and do not need to be identified with signals of possible $\omega$ bound states in nuclei.

In the MC calculations, we will impose the following cuts, for both the elementary $p(\gamma, \omega \to \pi^0\gamma)p$ and photonuclear $A(\gamma, \omega \to \pi^0\gamma)X$ reactions:

C1: The $\omega$ mesons are produced within an incident beam energy constrained by

$$1.5 < E_\gamma^{\text{in}} < 2.6 \quad \text{GeV}\,.$$

As in the actual experiment, the incident photons are distributed according to the unnormalized bremsstrahlung spectrum

$$W\left(E_\gamma^{\text{in}}\right) \sim \frac{1}{E_\gamma^{\text{in}}}. \tag{3}$$

C2: The polar angle $\theta_p$ of the protons produced via a quasifree kinematics is required to be detected in the range of

$$7^\circ < \theta_p < 14^\circ.$$

C3: To increase the number of $\omega \to \pi^0\gamma$ decays inside the nucleus, the three-momentum of the $\pi^0\gamma$ final state is restricted to values of

$$|\vec{p}_{\pi^0\gamma}| = |\vec{p}_{\pi^0} + \vec{p}_\gamma| < 400\,\text{MeV}.$$

Indeed, the fraction of the $\omega$ mesons decaying inside the nucleus can be optimized by minimizing the decay length $L_\omega = (p_\omega/m_\omega\Gamma_\omega)$, where $\Gamma_\omega$ is the width of the $\omega$ in the rest frame. It is therefore preferred that the kinetic energy of the $\omega$ mesons reconstructed from $\pi^0\gamma$ events with three-momenta $\vec{p}_\omega = \vec{p}_{\pi^0} + \vec{p}_\gamma$ is small.

C4: The kinetic energy $T_{\pi^0} = E_{\pi^0} - m_{\pi^0}$ of the detected $\pi^0$ is taken to be larger than 150 MeV. This cut will strongly suppress the distorted events due to the quasielastic $\pi^0$ final state interactions (FSI) with the nucleons of the target.

C5: The energy of the photon in the $\pi^0\gamma$ final state is larger than 200 MeV. This cut should attenuate the background channels and has negligible effect on the $\omega \to \pi^0\gamma$ signal as we shall see.

We start our MC analysis with the cross section of the elementary reaction $\gamma p \to \omega p \to \pi^0\gamma p$. In Ref. [43] the total cross section and the invariant differential cross sections $d\sigma_{\gamma p\to\omega p}/dt$ of the reaction $(\gamma, \omega)$ on protons were measured for incident photon energies from the reaction threshold $E_\gamma^{\text{th}} = m_\omega + m_\omega^2/2M_p \approx 1.1$ to 2.6 GeV. We use this experimental information in our analysis which is conveniently parametrized in Ref. [33]. In the following, the cross section on the neutron will be assumed to be the same as on a proton.

The results we are going to show, because of the cuts performed, rely upon $\omega$ production at backward angles in

$\gamma p \to \omega p$ in the center-of-mass frame. The experimental cross sections for this reaction are shown in Ref. [43], and one can see that there are large dispersions of the data at large angles, with also big changes from one energy to another. Our parametrization of Ref. [33] is good at small angles and rough at large angles. This means we necessarily have large uncertainties in the strength of the $\omega$ production, but, and this is the important thing, not in the shape. On the other hand, we do not make a detailed evaluation of the background either, although we shall estimate the contribution from two important channels. Thus, the exercise that we do here simply shows at a qualitative level, the relative change of the strength of the background to the $\omega$ signal for different nuclei. For this purpose, we do not need to have absolute values of the cross sections and we present our results in arbitrary units.

Our results for the differential cross section $d\sigma/dE_{\pi^0\gamma}$ as a function of $E_{\pi^0\gamma} - m_\omega$, where $E_{\pi^0\gamma} = E_{\pi^0} + E_\gamma$, and after applying the experimental cuts listed above, are shown in Fig. 8. There are preliminary data for this reaction from the CB-ELSA/TAPS experiment [35]. The lack of definitive data against which we could compare our results should not be an obstacle to discussing the theoretical results and drawing some conclusions. Apart from the cross section from $\gamma p \to \omega p \to \pi^0\gamma p$ that we evaluate, there should be background events from $\pi^0\gamma p$ events where the $\pi^0\gamma$ does not come from the decay of the $\omega$. These and other background events are certainly present in the reaction, as shown in Ref. [32], and they have larger strengths at invariant masses lower than $m_\omega$. There can also be other sources of background such as from $\gamma p \to \pi^0\pi^0 p$, or $\gamma p \to \pi^0\eta p$, where one of the two photons

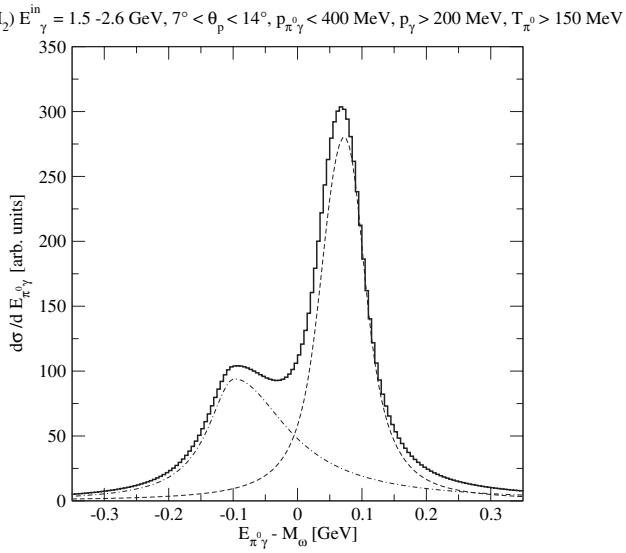


FIG. 8. Differential cross section $d\sigma/dE_{\pi^0\gamma}$ of the reaction $\gamma p \to \pi^0\gamma p$ as a function of $E_{\pi^0\gamma} - m_\omega$, where $E_{\pi^0\gamma} = E_{\pi^0} + E_\gamma$. The spectrum (solid histogram) is obtained using the reconstructed $\pi^0\gamma$ events from the exclusive $\gamma p \to \omega(\pi^0\gamma)p$ reaction (dashed curve) plus an inclusive $\pi^0\gamma$ background discussed in the text (dash-dotted curve). The following cuts were imposed: $E_\gamma^{\text{in}} =$ 1.5–2.6 GeV, $7^\circ < \theta_p < 14^\circ$, $|\vec{p}_{\pi^0} + \vec{p}_\gamma| < 400$ MeV, $|\vec{p}_\gamma| >$ 200 MeV, and $T_{\pi^0} >$ 150 MeV. The exclusive $\omega \to \pi^0\gamma$ signal has been folded with the 50 MeV experimental resolution.

from the decay of $\pi^0$ or $\eta$ is not measured, which should be more important. In fact, the phase space for the $\gamma p \to \pi^0\pi^0 p$ ($\pi^0 \to \gamma\gamma$) has indeed strength at lower $\pi^0\gamma$ invariant masses than $m_\omega$. To make this statement more concrete, we show in Fig. 9 the cross section $d\sigma/dE_{\pi^0\gamma}$ coming from the $\gamma p \to \pi^0\pi^0 p$ reaction followed by the decay $\pi^0 \to \gamma\gamma$ of either of the $\pi^0$ (left panel) and from the $\gamma p \to \pi^0\eta p$ reaction followed by the decay $\eta \to \gamma\gamma$ (right panel). The dashed curves are the event distributions when imposing cuts C1+C2. The dash-dotted and dash-dash-dotted curves are the results obtained after applying the experimental cuts C1+C2+C3 and C1+C2+C3+C4, respectively. Finally, when in addition to the previous cuts we restrict the final photon energy, as provided by cut C5, then both distributions (solid curves) are peaked at $E_{\pi^0\gamma} - M_\omega = -100$ MeV. Note that the units in Fig. 9 are absolute. We used the data for the $\gamma p \to \pi^0\pi^0 p$ reaction from Ref. [45], with a cross section of around 4.5$\mu$b in the region of interest to us, and the preliminary data for the $\gamma p \to \pi^0\eta p$ reaction from Ref. [46] ( see also published consistent data at lower energies in Ref. [47]) in order to estimate the relative cross sections of the $\pi^0\pi^0$ and $\pi^0\eta$ background processes. As one can see, the contribution from the $\pi^0\pi^0$ photoproduction to the background is the dominant one among the two. For this exercise, we abstained from doing an elaborate model and we simply took a constant transition $T$ matrix over the whole phase space in order to reproduce the value of the integrated cross sections for the reactions quoted above. A realistic choice of transition amplitude would somehow change the shape of the distributions obtained for $d\sigma/dE_{\pi^0\gamma}$, but it would not change the peak of the distribution which is given by the phase space for the reaction together with the imposed cuts. The important thing, thus, is that these two sources of background, with the cuts imposed, do indeed produce a background peaked at $-100$ MeV. It is curious and interesting to see that both reactions peak at the same place. This is of course an interesting finding from the experimental point of view, since logical improvements in the experiment should go into elimination of background sources, and the one from the $\gamma p \to \pi^0\pi^0 p$ reaction followed by the decay $\pi^0 \to \gamma\gamma$ is the first one to eliminate. The exercise done here shows that, even then, a smaller source of background with a similar shape would still remain from the $\gamma p \to \pi^0\eta p$ reaction followed by the decay $\eta \to \gamma\gamma$.

We do not want to make a complete theory of the background here, but simply justify that a background like the one assumed in Fig. 8, peaking around $m_\omega - 100$ MeV is rather plausible. On the other hand, with the admitted uncertainties in the strength of the $\omega$ signal, as discussed above, we obtain a factor of 2 bigger strength at the $\omega$ peak than at the peak from the $\gamma p \to \pi^0\pi^0 p$ background. Experimentally, this seems to be also the case from the preliminary data of the CB-ELSA/TAPS experiment, with a background very similar to that drawn in Fig. 8. Yet, the conclusions of this section are not tied to specific details of this background but to general features which we discuss below. In Fig. 8 the solid histogram is obtained as a sum of the reconstructed exclusive events from the $\gamma p \to \omega p \to \pi^0\gamma p$ reaction (dashed curve) and the background contribution. For the exclusive $\pi^0\gamma$ events coming from $\gamma p \to \omega p \to \pi^0\gamma p$, an experimental resolution of

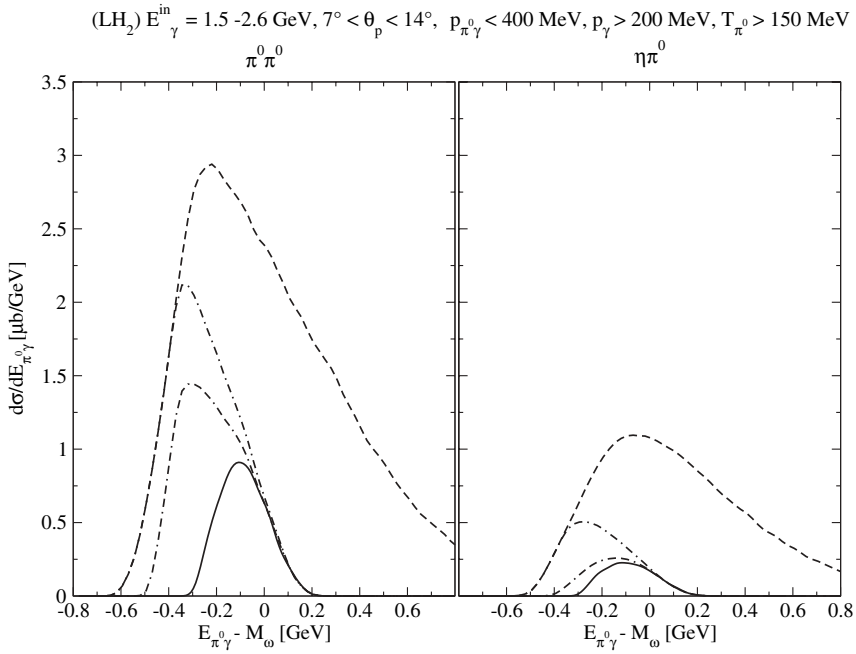


FIG. 9. Differential cross section $d\sigma/dE_{\pi^0\gamma}$ of the reactions $\gamma p \to \pi^0\pi^0 p$ (left panel) and $\gamma p \to \pi^0\eta p$ (right panel) followed by the decay $\pi^0(\eta) \to \gamma\gamma$ as a function of $E_{\pi^0\gamma} - m_\omega$, where $E_{\pi^0\gamma} = E_{\pi^0} + E_\gamma$. The following cuts were imposed: $E_\gamma^{\rm in} = 1.5$–2.6 GeV and $7^\circ < \theta_p < 14^\circ$ (dashed curves); $E_\gamma^{\rm in} = 1.5 - 2.6$ GeV, $7^\circ < \theta_p < 14^\circ$, and $|\vec{p}_{\pi^0} + \vec{p}_\gamma| < 400$ MeV (dash-dotted curves); plus the cut $T_{\pi^0} > 150$ MeV (dash-dash-dotted curves), and plus the cut $|\vec{p}_\gamma| > 200$ MeV (solid curves).

50 MeV was imposed, see Ref. [32]. Note that the last two cuts in the list, $E_\gamma > 200$ MeV and $T_{\pi^0} > 150$ MeV, are irrelevant for the $\omega \to \pi^0\gamma$ events since basically all of the MC events coming from this source fall in the kinematic regions allowed by these cuts.

In the photonuclear reaction $A(\gamma, \omega)X$, the $\omega$ mesons are produced inside the nucleus according to their in-medium spectral function which includes the collisional broadening of the $\omega$ due to the quasielastic and absorption channels. For the quasielastic scattering of $\omega$, we use the parametrization of the $\omega N \to \omega N$ cross section given in Refs. [14,22]. The in-medium quasielastic scattering does not lead to a loss of flux and therefore does not change the total nuclear cross section. But the latter affects the $\omega$ momentum and energy distributions, keeping the $\omega$ meson inside the nucleus for a longer time. The loss of $\omega$ flux is related to the absorptive part of the $\omega$-nucleus optical potential. In the following, the absorption width of the $\omega$ will be taken in the form

$$\Gamma_{\rm abs} \approx 100\,{\rm MeV} \times \frac{\rho(r)}{\rho_0}, \tag{4}$$

with no shift of the $\omega$ mass, as suggested by the analysis of Ref. [33], although this latter assumption is not relevant for the conclusions to be drawn. As will be shown in Ref. [44] (preliminary results are available in Ref. [35]), the in-medium $\omega$ width of $\simeq$100 MeV at normal nuclear matter density explains the nuclear transparency ratio measured in Ref. [35].

Using the MC method of Ref. [33], which proceeds in a close analogy to the actual experiment, we trace the fate of the $\omega$ mesons and their decay products in their way out of the nucleus. All standard nuclear effects such as Fermi motion of the initial nucleons and Pauli blocking of the final ones are taken into account. The $\omega$ mesons are allowed to propagate inside the nucleus, and at each step $\delta L$ the reaction probabilities for different channels such as the decay of the $\omega$ into $\pi^0\gamma$ and $\pi\pi\pi$ final states, quasielastic scattering, and in-medium absorption are properly calculated. Since we are interested in $\pi^0\gamma$ events, the absorption channels and decay $\omega \to \pi\pi\pi$ remove the $\omega$ mesons from the initial flux. The reconstructed $\pi^0\gamma$ events may come from the $\omega$ decaying both inside and outside the nucleus. If the resonance leaves the nucleus, its spectral function must coincide with the free distribution, because the collisional part of the width is zero in this case. When the $\omega$ decays into the $\pi^0\gamma$ pair inside the nucleus, its mass distribution is generated according to the in-medium spectral function at the local density. For a given mass $\tilde{m}_\omega$, the $\omega$ mesons are allowed to decay isotropically in the c.m. system into $\pi^0\gamma$ channel with a width $\Gamma_{\pi^0\gamma} =$ 0.76 MeV. The direction of the $\pi^0$ (therefore $\gamma$) is then chosen randomly, and an appropriate Lorentz transformation is done to generate the corresponding $\pi^0\gamma$ distributions in the laboratory frame. The $\omega$ mesons are reconstructed using the energy and momentum of the $\pi^0\gamma$ pair in the laboratory.

The reconstruction of the genuine $\omega \to \pi^0\gamma$ mode is affected by the final state interactions of the $\pi^0$ in the nucleus. In this case, if the $\pi^0$ events come from the interior of the nucleus, we trace the fate of the neutral pions starting from the decay point of the $\omega$ meson. On their way out of the nucleus, pions can experience quasielastic scattering or be absorbed. The intrinsic probabilities for these reactions as a function of the nuclear matter density are calculated using the phenomenological models of Refs. [48–50], which also include higher order quasielastic cuts and the two- and three-body absorption mechanisms. Note that the FSI of the pions distorts the $\pi^0\gamma$ spectra and makes an additional contribution to the negative part of the $E_{\pi^0\gamma} - m_\omega$ distribution. It was already demonstrated in Refs. [20,51] that the contributions of the distorted events due to the FSI of the pions can be largely suppressed by using the cut on kinetic energy of pions $T_\pi > 150$ MeV. We confirm this finding and use it further in our analysis. Since the FSI of the $\gamma$ quanta are rather weak, they are allowed to escape the nucleus without distortion.

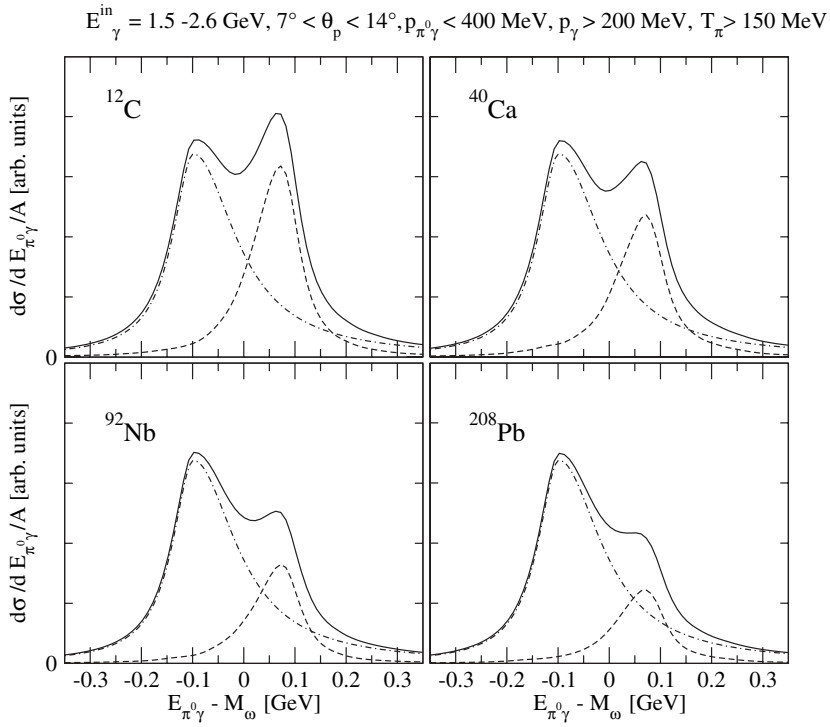


FIG. 10. Differential cross section $d\sigma/dE_{\pi^0\gamma}$ of the reaction $A(\gamma,\pi^0\gamma)X$ as a function of $E_{\pi^0\gamma} - m_\omega$ from $^{12}$C, $^{40}$Ca, $^{92}$Nb, and $^{208}$Pb nuclear targets. The reconstructed exclusive events from the $\omega \to \pi^0\gamma$ decay are shown by the dashed curves. The $\pi^0\gamma$ background is shown by the dash-dotted curves. The sum of the two contributions is given by the solid curves. The following cuts were imposed: $E^{\rm in}_\gamma = 1.5$–$2.6$ GeV, $7^\circ < \theta_p < 14^\circ$, $|\vec{p}_{\pi^0} + \vec{p}_\gamma| < 400$ MeV, $|\vec{p}_\gamma| > 200$ MeV, and $T_\pi > 150$ MeV. The exclusive $\omega \to \pi^0\gamma$ signal has been folded with the 50 MeV experimental resolution. All spectra are normalized to the corresponding nuclear mass numbers $A$.

## IV. RESULTS OF THE MC CALCULATIONS

In the following, we assume that the inclusive $\pi^0\gamma$ background scales with respect to the target nucleus mass number $A$ as

$$\sigma_A \approx A\sigma_{\rm elem}. \tag{5}$$

This assumption implies merely a rather weak absorption of the inclusive $\pi^0\gamma$ pairs in the nuclear medium. Note that this assumption is supported by the present MC calculations which show only the marginal effects due to the FSI of the relatively fast pions [beyond the $\Delta(1232)$ region]. Recall that because of the cuts we have imposed, the kinetic energies of the pions are always larger than $T_\pi > 150$ MeV. But this is not the case for the exclusive $\pi^0\gamma$ events coming from the decay of the $\omega \to \pi^0\gamma$. Although the pions coming from this source are also fast and easily abandon the nucleus without significant FSI, the rather strong absorption of the $\omega$ inside the nucleus might change the scaling relation Eq. (5) and

$$\sigma_A(\omega \to \pi^0\gamma) \approx A^\alpha\, \sigma_{\rm elem}(\omega \to \pi^0\gamma), \tag{6}$$

where the attenuation parameter $\alpha < 1$.

In Fig. 10, we show the results of the MC simulation for the $E_{\pi^0\gamma} - m_\omega$ spectra reconstructed from the $\pi^0$ and $\gamma$ events. The calculations are performed for the sample nuclear targets $^{12}$C, $^{40}$Ca, $^{92}$Nb, and $^{208}$Pb. The kinematic and acceptance cuts discussed before have been already imposed. The MC distributions are normalized to the nuclear mass number $A$. The solid curves correspond to the sum of the inclusive $\pi^0\gamma$ background (dash-dotted curve), which is not related to the production and decay of the $\omega$ mesons and the exclusive $\pi^0\gamma$ events coming from the direct decay of the $\omega \to \pi^0\gamma$. The contributions of the exclusive $\omega \to \pi^0\gamma$ events are shown by the dashed curves. We note a very strong attenuation of the $\omega \to \pi^0\gamma$ signal with respect to the background contribution with increasing nuclear mass number $A$. This is primary due to the stronger absorption of the $\omega$ mesons with increasing nuclear matter density, see Eq. (4). Also the contribution of the $\omega$ mesons decaying inside the nucleus (with and without $\pi^0$ rescattering) is increasing as a function of mass number $A$ merely because of an increase in the effective radius of the nucleus.

The former exercise indicates that given the particular combination of $\pi^0\gamma$ from an uncorrelated background and from $\omega$ decay, and the different behavior of these two sources in the $\pi^0\gamma$ production in nuclei, a double hump structure seems unavoidable in nuclei unless further efforts are made to subtract the background. Had we not performed this calculation and interpreted it in the way we have done, the observation of a peak at about 100 MeV below the $\omega$ mass could easily tempt anyone to claim it as an indication of an $\omega$ bound state in the nucleus. By performing the present study, we have paved the way for future investigations on the topic with the performance of the necessary simulation of conventional mechanisms which accompany the reactions used in the search for more exotic phenomena. Obviously, removal of different background sources would be another way to proceed.

We would like to insist on considering the issue of the background, because there can be many sources for it. In the CB-ELSA/TAPS experiment, where $\pi^0$ is observed from the two $\gamma$ decay, a background of $\pi^0\gamma$ could also come from the production of two $\pi^0$ or $\pi^0\eta$, with no detection of a fourth $\gamma$ coming from one $\pi^0$ or $\eta$ decay. Such background could be eliminated, but there are unavoidable backgrounds like that coming from the $\gamma p \to p\pi^0\gamma$ reaction. Having this in mind,

it is worth mentioning that, even if the background of the reaction after eliminating avoidable backgrounds is about one third of the one assumed in the present discussion, or even smaller, a two bump structure like the one of Fig. 10 will still show up.

Finally, we would like to make a final comment in the sense that the strength of the cross section bears some information in itself. In the calculations done for the capture of $\omega$ mesons in bound orbits, the cross sections are presented in absolute numbers. Should experiments find some peak structure in the $\omega$ bound region with a strength considerably larger than the one predicted in the present calculations, this would be an indication that the strength observed is coming from some sort of background, not from the formation of $\omega$ bound states.

## V. CONCLUSIONS

In the present work we have carried out some calculations that should be very helpful in the search for eventual $\omega$ bound states in nuclei. In the first part, we evaluated the reaction cross sections for the $(\gamma, p)$ reaction in nuclei leading to the production of bound or unbound $\omega$ states together with the excitation of nuclear bound states. The calculations were done using different optical potentials which covered a wide range of bindings and absorptive parts. We found that only for potentials where the real part was larger than twice the imaginary part was there some chance to see peaks in the $\omega$ energy spectrum corresponding to the formation of the $\omega$ bound states. Clear peaks could be seen for a potential $(-156, -29)$ MeV (at $\rho = \rho_0$), while if we had an imaginary part of about $-50$ MeV, as suggested by present experimental data on the $A$ dependence of $\omega$ production, even with 100 MeV binding, no signal could be seen in the calculated spectrum. We studied the reaction for different photon energies and different proton angles. Since the optimal situation to see the peaks appears for recoilless kinematics, the photon energy of 2 GeV was the optimal one if one observes protons in the forward direction. However, if the experimental conditions make it impossible or difficult to measure forward protons and a proton angle around $10^\circ$ is the choice, then we showed that a photon energy of about 1.2 GeV was more suited and led to better recoilless kinematics than with photons of 2 GeV. We performed the calculations for this situation which should serve to compare with experimental measurements made in the future.

Another relevant finding of the present work was that even if bound states exist and they lead to peaks in the $(\gamma, p)$ reaction, an experimental resolution better than 20 MeV in the $\omega$ energy is mandatory to make the peaks visible.

Finally we made another useful evaluation by calculating the inclusive $(\gamma, p)$ reaction leading to $\pi^0\gamma$ events. To the elementary reaction $\gamma p \to \omega p$ with subsequent $\pi^0\gamma$ decay of the $\omega$ we added a certain background from reactions leading to $\pi^0\gamma$ with no connection to $\omega$ production. Then we studied this reaction in nuclei, and because of the different behavior in the production of uncorrelated and $\omega$ correlated $\pi^0\gamma$ pairs, we showed that a peak appeared in nuclei in the region of $\pi^0\gamma$ energy around $m_\omega - 100$ MeV, which could easily be misidentified by a signal of a bound $\omega$ state in nuclei.

Altogether, the information found here should be of much help in identifying the ideal setups for future experiments searching for $\omega$ bound states in nuclei and in properly interpreting the results of those experiments.

## ACKNOWLEDGMENTS

We would like to acknowledge useful discussions with V. Metag, M. Kotulla, and D. Trnka. One of the authors (H.N.) is supported by a Research Fellowship of JSPS for Young Scientists. This work is partly supported by DGICYT Contract No. FIS2006-03438, the EU Integrated Infrastructure Initiative Hadron Physics Project under Contract No. RII3-CT-2004-506078, the Grants-in-Aid for scientific research of JSPS [No. 16540254 (S.H.) and No. 18-8661 (H.N.)], and by CSIC and JSPS under the Spain-Japan Research Cooperative Program.

[1] M. Post, S. Leupold, and U. Mosel, Nucl. Phys. **A741**, 81 (2004).
[2] G. E. Brown and M. Rho, Phys. Rev. Lett. **66**, 2720 (1991).
[3] T. Hatsuda and S. H. Lee, Phys. Rev. C **46**, R34 (1992).
[4] V. Bernard and U. G. Meissner, Nucl. Phys. **A489**, 647 (1988).
[5] H. Kurasawa and T. Suzuki, Prog. Theor. Phys. **84**, 1030 (1990).
[6] H. C. Jean, J. Piekarewicz, and A. G. Williams, Phys. Rev. C **49**, 1981 (1994).
[7] F. Klingl, N. Kaiser, and W. Weise, Nucl. Phys. **A624**, 527 (1997).
[8] K. Saito, K. Tsushima, A. W. Thomas, and A. G. Williams, Phys. Lett. **B433**, 243 (1998).
[9] K. Tsushima, D. H. Lu, A. W. Thomas, and K. Saito, Phys. Lett. **B443**, 26 (1998).
[10] B. Friman, Acta Phys. Pol. B **29**, 3195 (1998).
[11] F. Klingl, T. Waas, and W. Weise, Nucl. Phys. **A650**, 299 (1999).
[12] M. Post and U. Mosel, Nucl. Phys. **A688**, 808 (2001).
[13] K. Saito, K. Tsushima, D. H. Lu, and A. W. Thomas, Phys. Rev. C **59**, 1203 (1999).
[14] G. I. Lykasov, W. Cassing, A. Sibirtsev, and M. V. Rzyanin, Eur. Phys. J. A **6**, 71 (1999).
[15] A. Sibirtsev, C. Elster, and J. Speth, arXiv:nucl-th/0203044 (unpublished).
[16] A. K. Dutt-Mazumder, R. Hofmann, and M. Pospelov, Phys. Rev. C **63**, 015204 (2001).
[17] M. F. M. Lutz, G. Wolf, and B. Friman, Nucl. Phys. **A706**, 431 (2002); **A765**, 431(E) (2006).
[18] S. Zschocke, O. P. Pavlenko, and B. Kampfer, Phys. Lett. **B562**, 57 (2003).
[19] A. K. Dutt-Mazumder, Nucl. Phys. **A713**, 119 (2003).
[20] P. Muhlich, T. Falter, and U. Mosel, Eur. Phys. J. A **20**, 499 (2004).
[21] P. Muehlich, V. Shklyar, S. Leupold, U. Mosel, and M. Post, Nucl. Phys. **A780**, 187 (2006).
[22] P. Muhlich and U. Mosel, Nucl. Phys. **A773**, 156 (2006).
[23] B. Steinmueller and S. Leupold, Nucl. Phys. **A778**, 195 (2006).

[24] R. Arnaldi *et al*. (NA60 Collaboration), Phys. Rev. Lett. **96**, 162302 (2006).
[25] M. Naruki *et al*., Phys. Rev. Lett. **96**, 092301 (2006).
[26] C. Djalili, talk at Yukawa Symposium, Kyoto, December 2006 (unpublished).
[27] U. Mosel, Prog. Part. Nucl. Phys. **42**, 163 (1999).
[28] K. Ozawa *et al*. (E325 Collaboration), Phys. Rev. Lett. **86**, 5019 (2001).
[29] T. Tabaru *et al*., Phys. Rev. C **74**, 025201 (2006).
[30] F. Sakuma *et al*. (E325 Collaboration), Phys. Rev. Lett. **98**, 152302 (2007).
[31] D. Weygand, talk at the QNP06 Conference, Madrid, June 2006.
[32] D. Trnka *et al*. (CB-ELSA/TAPS Collaboration), Phys. Rev. Lett. **94**, 192303 (2005).
[33] M. Kaskulov, E. Hernandez, and E. Oset, Eur. Phys. J. A **31**, 245 (2007).
[34] E. Marco and W. Weise, Phys. Lett. **B502**, 59 (2001).
[35] D. Trnka, Ph.D. thesis, University of Giessen, 2006.
[36] R. S. Hayano, S. Hirenzaki, and A. Gillitzer, Eur. Phys. J. A **6**, 99 (1999).
[37] O. Morimatsu and K. Yazaki, Nucl. Phys. **A435**, 727 (1985); **A483**, 493 (1988).
[38] D. Jido, H. Nagahiro, and S. Hirenzaki, Phys. Rev. C **66**, 045202 (2002); H. Nagahiro, D. Jido, and S. Hirenzaki, *ibid*. **68**, 035205 (2003); Nucl. Phys. **A761**, 92 (2005).
[39] H. Nagahiro, M. Takizawa, and S. Hirenzaki, Phys. Rev. C **74**, 045203 (2006).
[40] H. Toki, S. Hirenzaki, and T. Yamazaki, Nucl. Phys. **A530**, 679 (1991); S. Hirenzaki, H. Toki, and T. Yamazaki, Phys. Rev. C **44**, 2472 (1991).
[41] S. Hirenzaki and E. Oset, Phys. Lett. **B527**, 69 (2002).
[42] H. Gilg *et al*., Phys. Rev. C **62**, 025201 (2000); K. Itahashi *et al*., *ibid*. **62**, 025202 (2000); H. Geissel *et al*., Phys. Rev. Lett. **88**, 122301 (2002); K. Suzuki *et al*., *ibid*. **92**, 072302 (2004).
[43] J. Barth *et al*., Eur. Phys. J. A **18**, 117 (2003).
[44] D. Trnka *et al*. (to be published).
[45] U. Thoma, Int. J. Mod. Phys. A **20**, 280 (2005).
[46] M. Nanova, in *NSTAR 2005: Proceedings of the Workshop on the Physics of Excited Nucleons*, edited by S. Capstick, Volker Crede, Paul Michael Eugenio (World Scientific, Singapore, 2006).
[47] T. Nakabayashi *et al*., Phys. Rev. C **74**, 035202 (2206).
[48] L. L. Salcedo, E. Oset, M. J. Vicente-Vacas, and C. Garcia-Recio, Nucl. Phys. **A484**, 557 (1988).
[49] E. Oset, L. L. Salcedo, and D. Strottman, Phys. Lett. **B165**, 13 (1985).
[50] E. Oset and D. Strottman, Phys. Rev. C **42**, 2454 (1990).
[51] J. G. Messchendorp, A. Sibirtsev, W. Cassing, V. Metag, and S. Schadmand, Eur. Phys. J. A **11**, 95 (2001).